J|A|C|S
ARTICLES
Published on Web 02/27/2003

NMR Structure of Two Novel Polyethylene Glycol Conjugates of the Human Growth Hormone-Releasing Factor, hGRF(1−29)−NH_2

Giuseppe Digilio,*,† Luca Barbero,‡ Chiara Bracco,†,§ Davide Corpillo,†,§ Pierandrea Esposito,‡ Gilles Piquet,‡ Silvio Traversa,‡ and Silvio Aime§

Contribution from the Bioindustry Park del Canavese, Via Ribes 5, I-10010 Colleretto Giacosa (TO), Italy, Istituto di Ricerca Cesare Serono—Drug Delivery Systems; Via Ribes 5, I-10010, Colleretto Giacosa (TO), Italy, and Department of Chemistry I.F.M., University of Turin, Via P. Giuria 7, I-10125 Turin, Italy

Received October 8, 2002; Revised Manuscript Received December 10, 2002; E-mail: chemlima@bioindustrypark.it.

Abstract: Two novel mono-PEGylated derivatives of hGRF(1−29)−NH_2 [human growth hormone-releasing factor, fragment 1−29] have been synthesized by regio-specific conjugation of Lys^{12} or Lys^{21} to a monomethoxy-PEG_{5000} chain (compounds Lys^{12}PEG−GRF and Lys^{21}PEG−GRF). The PEG moiety has been covalently linked at the amino group of a norleucine residue via a carbamate bond. The Lys^{12}PEG−GRF regioisomer was found to be slightly less active in vitro than both the unmodified peptide and Lys^{21}PEG−GRF. To assess whether the differences in the biological activity of the PEGylated analogues could be related to conformational rearrangements induced by the PEG moiety, the structure of these PEGylated derivatives has been worked out (TFE solution) by means of NMR spectroscopy and molecular dynamics. Secondary structure shifts, hydrogen/deuterium exchange kinetics, temperature coefficients of amide protons, and NOE-based molecular models point out that hGRF(1−29)−NH_2, Lys^{21}PEG−GRF and Lys^{12}PEG−GRF share a remarkably similar pattern of secondary structure. All three compounds adopt an α-helix conformation which spans the whole length of the molecule, and which becomes increasingly rigid on going from the N-terminus to the C-terminus. Residues Lys^{12} and Lys^{21} are enclosed in all the compounds considered into well-defined α-helical domains, indicating that PEGylation either at Lys^{12} or Lys^{21} does not alter the tendency of the peptide to adopt a stable α-helix conformation, nor does it induce appreciable conformational mobility in the proximity of the PEGylation sites. No significant variation of the amphiphilic organization of the α-helix is observed among the three peptides. Therefore, the different biological activities observed for the PEGylated analogues are not due to conformational effects, but are rather due to sterical hindrance effects. The relationship between the biological activitiy of the mono-PEGylated derivatives and sterical hindrance is discussed in terms of the topology of interaction between hGRF(1−29)−NH_2 and its receptor.

Introduction

The chemical modification of proteins through the conjugation to one or more functionalized monomethoxypoly(ethyleneglycol) units (PEG) has proven to be a valuable route for the development of analogues endowed with improved pharmacological properties, including a better resistance to proteolytic cleavage, higher solubility in physiological media, longer plasma half-life, and decreased immunogenicity.[1−3] The site of conjugation to PEG must be carefully chosen to avoid a loss of intrinsic biological activity which may vanish the advantages due to the enhancement of the duration of activity. As a matter of fact, PEG units may block critical sites for the molecular recognition process because of sterical hindrance (PEG units with a molecular mass ranging from 2 up to 20 KDa are usually employed). For smaller proteins or peptides, whose bioactive fold is not stabilized by tertiary structure interactions, an additional cause of the loss of intrinsic potency may be ascribed to conformational changes brought about by the PEG moieties. This effect is expected to become more important as the molecular weight of the peptide decreases.

The site-directed PEGylation strategy is nevertheless becoming very attractive also in the field of bioactive peptides, and it has been successfully employed to enhance the pharmacolgical properties of fragment 1−29 of the human growth hormone-releasing factor [hGRF(1−29)−NH_2][4,5] and analogues.[6,7] The hGRF(1−29)−NH_2 fragment has been shown to be the shortest

† Bioindustry Park del Canavese.
‡ Istituto di Ricerca Cesare Serono—Drug Delivery Systems.
§ Department of Chemistry I.F.M., University of Turin.

(1) (a) Nucci, M. L.; Shorr, R.; Abuchowski, A. *Adv. Drug Delivery Rev.* **1991**, *6*, *133*−151. (b) Roberts, M. J.; Bentley, M. D.; Harris, J. M. *Adv. Drug Delivery Rev.* **2002**, *54*, *459*−476. (c) Wang, Y.-S.; Youngster, S.; Grace, M.; Bausch, J.; Bordens, R.; Wyss, D. F. *Adv. Drug Delivery Rev.* **2002**, *54*, *547*−570.
(2) Ho, D. H.; Brown, N. S.; Yen, A.; Holmes, Y. R.; Keating, M.; Abuchowski, A.; Newman, R. A.; Krakoff, I. H. *Drug Metab. Dispos.* **1986**, *14*, 349−352.
(3) Katre, N. V.; Knauf, M. J.; Laird, W. J. *Proc. Natl. Acad. Sci. U.S.A.* **1987**, *84*, 1487−1491.

10.1021/ja021264j CCC: $25.00

fragment of native hGRF [hGRF(1−44)−NH$_2$] retaining a significant GH-releasing activity.[8−10] The potency of the PEGylated analogues was found to be strongly dependent upon the site of PEGylation. PEGylation at the C-terminus of hGRF-(1−29)−NH$_2$ and a number of analogues was shown not to affect the in vitro biological activity with respect to the parent non-PEGylated compounds, whereas the duration of activity of the PEGylated derivatives was greatly enhanced in vivo because of a reduced clearance from blood and tissues.[6] PEGylation at position Lys^{21} or Asp^{25} of the highly potent [Ala^{15}]-hGRF-(1−29)−NH$_2$ analogue did not significantly affect the in vitro potency relative to the un-PEGylated peptide regardless of the molecular weight of PEG. On the other hand, PEGylation at Lys^{12} or Asp^{8} caused a sharp decrease of the in vitro biological potency and such a decrease was dependent upon the molecular weight of the PEG unit.[7] PEGylation at the amino-terminus of [Ala^{15}]-hGRF(1−29)−NH$_2$ also yielded a loss of GH-releasing activity, which was however comparable to the potency decrease observed for the N-terminus acetylated [Ala^{15}]-hGRF(1−29)−NH$_2$. Hindered binding to the receptor may be not the only explanation for the observed behavior of PEGylated hGRF-(1−29)−NH$_2$ analogues and other effects such as conformational ones can have a key contribution to the receptorial affinity. Moreover, it has been proposed that the modification of the amphiphilic character of hGRF(1−29)−NH$_2$ can severely modify the interaction between the ligand and the cell membrane, and ultimately affect the receptor binding affinity.[11,12] The relevance of conformational effects toward the biological potency of hGRF and its analogues is highlighted by CD and NMR structural investigations. Native hGRF(1−29)−NH$_2$ has been shown by NMR and CD studies to have a degree of α-helix content as low as 20% in water solution,[12,13,14] but the content of α-helix increased up to 90% when structure-promoting solvents were used (methanol/water 75% and TFE/water 30%).[15,16] Interestingly, the intrinsic potency of hGRF(1−29)−NH$_2$ analogues appeared to correlate with their content of α-helical structure. Replacement of Gly^{15} with α-helix stabilizing residues (Ala, Aib) afforded analogues showing a 4-fold increase of potency in vitro ([Ala^{15}]-hGRF(1−29)−NH$_2$ is 5−6-fold more potent than hGRF(1−44)−NH$_2$ in vivo).[12] Conversely, substitution of Gly^{15} with Sar^{15} (an α-helix destabilizing residue) abolished the receptor binding affinity and GH-releasing activity.[12] Structural investigations confirmed that the [Ala^{15}]-hGRF(1−29)−NH$_2$ analogue was largely α-helical, because Ala^{15} was found to extend the length of the α-helix fragments to encompass the central peptide region. On the other hand, the [Sar^{15}]-GRF(1−29)−NH$_2$ showed little evidence of ordered secondary structure.[13] Conformational studies carried out on covalently constrained mono- and polycyclic analogues of hGRF(1−29)−NH$_2$ also supported the view that GRF binding affinity to its receptor increases as the extent and stability of α-helix structure increase.[7,17]

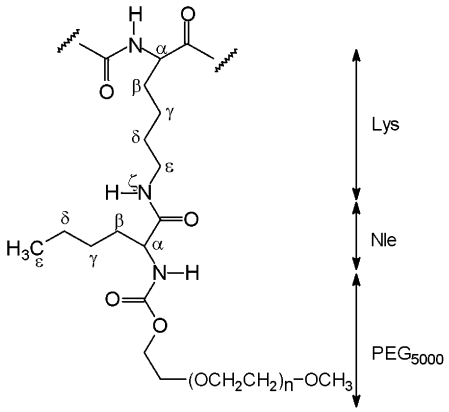

Figure 1. Schematic representation of the covalent structure of the Nε−[monomethoxy(polyethyleneglycol)norleucyl]lysine moiety.

In this paper, we describe the NMR conformational analysis of two new derivatives of hGRF(1−29)−NH$_2$ which were conjugated at Lys^{12} or Lys^{21} to a PEG$_{5000}$ unit through a Nle spacer (compounds Lys^{12}PEG−GRF and Lys^{21}PEG−GRF, Figure 1). The scope of this study is to assess whether PEGylation of hGRF(1−29)−NH$_2$ introduces conformational rearrangements which can be related to changes in the biological potency. Because the tendency of hGRF to form stable secondary structures is more easily studied in structure promoting solvents rather than in aqueous solution,[18,19,20] NMR experiments were carried out in neat TFE. The conformation of native hGRF-(1−29)−NH$_2$ in TFE solution has been determined as well in order to obtain a reference structural model.

Methods

Synthesis of Lys^{12}PEG−GRF and Lys^{21}PEG−GRF. The synthesis and characterization of the PEGylated derivatives of hGRF(1−29)−NH$_2$ has been described in detail elsewhere.[4,5] The identity and purity of the conjugates were assessed by using RP-HPLC on a 4.6 × 250 mm, 5μm, 300A, C5 Jupiter column (Phenomenex). Eluents contained water, acetonitrile and 2-propanol as organic phase and trifluoroacetic acid as ion pairing reagent. By means of a linear gradient elution, the two peaks were resolved at a baseline level with a resolution at half-height of 13. Identity was confirmed by injection of pure standards of Lys^{21}PEG−GRF and Lys^{12}PEG−GRF and by comparing the retention times. Purity was assessed by injection of purified couples of mono-

(4) Caliceti, P.; Schiavon, O.; Veronese, F. M. WO Patent 99/27897 1999; *Chem. Abstr.* **1999**, *131*, 19 307.
(5) Piquet, G.; Barbero, L.; Traversa, S.; Gatti, M. WO Patent 02/28437 2002; *Chem. Abstr.* **2002**, *136*, 295 095.
(6) Campbell, R. M.; Heimer, E. P.; Ahmad, M.; Eisenbeis, H. G.; Lambros, T. J.; Lee, Y. Miller, R. W.; Stricker, P. R.; Felix, A. M. *J. Peptide Res.* **1997**, *49*, 527−537.
(7) Felix, A. M.; Lu, Y. A.; Campbell, R. M. *Int. J. Peptide Protein Res.* **1995**, *46*, 253−264.
(8) Ling, N.; Baird, A.; Wehrenberg, W. B.; Ueno, N.; Munegumi, T.; Brazeau, P. *Biochem. Biophys. Res. Commun.* **1984**, *123*, 854−861.
(9) Campbell, R. M.; Lee, Y.; Mowles, T. F.; Melntyre, K. W.; Ahmad, M.; Felix, A. M.; Heimer, E. P. *Peptides* **1992**, *13*, 787−793.
(10) Campbell, R. M.; Lee, Y.; Rivier, S.; Heimer, E. P.; Felix, A. M.; Mowles, T. F. *Peptides* **1991**, *12*, 569−574.
(11) Kaiser, E. T.; Kezdy, F. J. *Science* **1984**, *223* (4633), 249−255.
(12) Campbell, R. M.; Bongers, J.; Felix, A. M. *Biopolymers (Peptide Sci.)* **1995**, *37*, 67−88.
(13) Madison, V.; Berkovitch-Yellin, Z.; Fry, D.; Greeley, D.; Toome, V. in *Synthetic Peptides: Approaches to Biological Problems*; Tam, J., Kaiser, E. T., Eds.; Alan R. Liss Inc, 1989, pp. 109−123.
(14) Madison, V. S.; Fry, D. C.; Wegrzynski, B. B.; Williamson, M. P.; Campbell, R. M.; Danho, W.; Heimer, E. P.; Felix, A. M. In *Proteins: Structures, Dynamics and Design*; Renugopalakrishnan, V., Carey, P. R., Smith, I. C. P., Huang, S. G., Storer, A. C., Eds.; ESCOM Publishers BV: Leiden, 1991, pp 234−239.
(15) Clore, G. M.; Martin, S. R.; Gronenborn, A. M. *J. Mol. Biol.* **1986**, *191*, 553−561.
(16) Brünger, A. T.; Clore, G. M.; Gronenborn, A. M.; Karplus, M. *Protein Eng.* **1987**, *1* (5), 399−406.
(17) Fry, D.; Madison, V. S.; Greely, D. N.; Felix, A. M.; Heimer, E. P.; Frohman, L.; Campbell, R. M.; Mowles, T. F.; Toome, V.; Wegrzynski, B. B. *Biopolymers* **1992**, *32*, 649−666.
(18) Cammers-Goodwin, A.; Allen, T. J.; Oslick, S. L.; McClure, K. F.; Lee, J. H.; Kemp, D. S. *J. Am. Chem. Soc.* **1996**, *118*, 3082−3090.
(19) Walgers, R.; Lee, T. C.; Cammers-Goodwin, A. *J. Am. Chem. Soc.* **1998**, *120*, 5073−5079.
(20) Najbar, L. V.; Craik, D. J.; Wade, J. D.; Salvatore, D.; McLeish, M. J. *Biochemistry* **1997**, *36*, 11 525−11 533.

PEGylated species at Lys^{21} and Lys^{12} of the main degraded forms of hGRF(1−29)−NH_2, i.e., β-[Asp^3]-hGRF(1−29)NH_2, [Asp^8]-hGRF-(1−29)NH_2, β-[Asp^8]-hGRF(1−29)NH_2, [$Met(O)^{27}$]-hGRF(1−29)NH_2, hGRF(3−29)NH_2, and hGRF(1−29)OH. The peaks coming from these degraded forms of Lys^{21}PEG−GRF and Lys^{12}PEG−GRF were separated at a baseline level from the peaks of intact Lys^{21}PEG−GRF and Lys^{12}PEG−GRF. The average molecular weight for both Lys^{21}PEG−GRF and Lys^{12}PEG−GRF is 8763 Da (MALDI-TOF mass spectrometry).

NMR Spectroscopy. The concentration of peptide in TFE-d_2−OH solution (Isotec, 99.8% atom D) and TFE-d_3 solution (Aldrich, 99.5% atom D) was 8.5 mg/mL for hGRF(1−29)−NH_2 (Bachem AG, CH) and 5.0 mg/mL for the PEGylated analogues (corresponding to 2.5 mmol/L and 0.6 mmol/L respectively). NMR spectra were acquired at temperatures ranging from 290 K to 320 K. ^{1}H chemical shifts were referenced to TMS by using the CF_3−CHD−OD signal as a secondary standard. Aqueous samples were prepared by dissolving hGRF(1−29)−NH_2 (3.3 mg/mL) or the PEGylated analogues (4.0 mg/mL) in doubly distilled water (550 μL) and adding D_2O (50 μL, Isotec, 99.8% atom D) for the field-frequency lock. The pH was in the range 4.7−5.4 (pH meter reading, uncorrected for the isotope effect). 2D-NMR spectra of aqueous solutions were acquired at 275 and 280 K and ^{1}H chemical shifts were referenced to external TMS.

NMR experiments were carried out on a Bruker Avance 600 spectrometer operating at 14 T (corresponding to a proton Larmor frequency of 600 MHz) equipped with a triple axis-PFG probe optimized for the detection of the ^{1}H nucleus. 2D-TOCSY experiments were carried out by means of the MLEV17 pulse sequence for isotropic mixing with a duration of 80−100 ms and a spin-locking field strength of 10 kHz. The TPPI phase cycling method was used to obtain complex data points in the t_1 dimension. 2D-NOESY experiments were carried out by the standard pulse sequence with the hypercomplex (STATES-TPPI) phase cycling scheme; mixing times ranging from 60 to 350 ms have been used. Solvent suppression was achieved in the case of TFE-d_2−OH samples by means of presaturation of the solvent line during the recycle delay in both TOCSY and NOESY spectra. The strong signal from PEG ethyleneglycol groups at about 3.7 ppm was also suppressed by selective presaturation during the recycle delay. In the case of aqueous samples, solvent suppression has been achieved by means of the PFG-WATERGATE technique. 2D-DQF-COSY experiments were obtained in the phase sensitive mode by the hypercomplex (STATES-TPPI) method with the standard double quantum filtered pulse sequence. The attenuation of the signal from TFE-d_2−OH was obtained by means of the presaturation technique, whereas no suppression of the resonance of PEG methylene groups was done.

Typical experimental settings for 2D-NMR experiments included: spectral width 6009 Hz (both F_2 and F_1 dimensions), recycle delay 2.5s, 2048 and 512 complex data points for the t_2 and t_1 dimensions respectively, 32 to 64 scans for t_1 increment. The data were apodized with a square cosine window function and zero filled to a matrix of size 1024 × 1024 prior to Fourier transformation and baseline correction.

For hydrogen/deuterium exchange experiments, aliquots of solid hGRF(1−29)−NH_2 (1.26 mg) or of the PEGylated analogues (3.0 mg) were weighted into a 5 mm NMR tube and quickly dissolved into neat TFE-d_3 (600μL). The instrumental settings were preadjusted on a dummy sample to minimize the time between the addition of the solvent and the acquisition of the first ^{1}H NMR spectrum. The time interval was about 5 min. All of the exchange experiments were performed at a temperature of 310 K. The assignment of the decaying amide signals was achieved by recording monodimensional ^{1}H NMR spectra within a time interval of 2 days and by means of TOCSY and NOESY experiments (acquired at about 250 and 1100 min after dissolution). These 2D-NMR experiments were carried out with essentially the same instrumental settings as described above, except that 256 complex data points were collected in the t_1 dimension.

Molecular Dynamics and Energy Minimization. All calculations were carried out on a Silicon Graphics Octane workstation. The assignment of NMR signals and integration of NOE peaks were done by means of the XEASY[21] software package. The assignment of ^{1}H NMR resonances was carried out by the sequence-specific method,[22] i.e., by iterative comparison of TOCSY, NOESY and DQF-COSY spectra. A number of ambiguities in the assignment due to severe signal overlap could be resolved by comparing experiments carried out at different temperatures. The structure optimization based on NMR constraints was carried out by the program DYANA[23] (energy minimization by torsion angle dynamics and simulated annealing) and structure analysis by means of MOLMOL[24] (molecular graphics). Peak volumes were obtained from NOESY spectra acquired with mixing times of 250−300 ms. Upper distance limits involving diastereotopic atom pairs without stereospecific assignment were increased in order to allow for both assignments as described in ref 25. To account for the effect of local motions on the intensity of the NOE signals, the peak volume-to-internuclear upper limit bound conversion was executed by classifying the NOEs into three different calibration classes and applying to each of them a different calibration function, following the DYANA standard procedure. The solution structures of hGRF-(1−29)−NH_2 and PEGylated analogues were optimized by means of molecular dynamics in the torsion angle space (torsion angle dynamics, TAD) and simulated annealing. Typically, one thousand conformers with random values of both backbone and side-chain dihedral angles were generated (bond length and bond angles were fixed at their optimal values according to the ECEPP/2[26] standard geometry). DYANA minimizations were carried out with 5000 TAD steps, and the contribution to the target function due to the violation of the upper limit distance constraints was calculated according to a square potential function. The optimized conformers were accepted if their residual target function was below the cutoff value of 0.56 Å^2 and if they did not present any consistent steric or geometric violation. A sub-ensemble of structures endowed with lowest target function values (typically 30) was extracted from the ensemble of acceptable ones for further structural analyses. The PEG_{5000}−Nle moiety was not explicitly included in the TAD calculations [i.e., constrained molecular dynamics were carried out on the hGRF(1−29)−NH_2 molecule]. Energy minimization and Monte Carlo Conformational Search (MC CS) calculations were performed with the MACROMODEL 6.5 software package (Columbia University, NY).[27] These calculations were done with the AMBER* force field.[28] Thirty optimized structures of Lys^{21}PEG−GRF obtained from restrained TAD with simulated annealing were forwarded to the MACROMODEL software package, added with a Nα-carbomethoxy-L-norleucyl fragment at the amino group of Lys^{21} and subjected to 500 iteration molecular mechanics cycles, using the Polak−Ribiere conjugate gradient minimization mode. The value of the derivative convergence criterion was 0.5 KJ·mol^{-1} Å^{-1}. Energy minimizations were performed in vacuo. The analysis of the possible conformations at the PEG_{5000}−Nle fragment was performed by MC CS followed by further energy minimization. In all calculations, χ_3, χ_4, χ_5 dihedral angles of Lys^{21}, ϕ, ψ, and side chain χ angles of Nle, and the C(O)−OCH_3

(21) Bartels, C. H.; Xia, T.-H.; Billeter, M.; Güntert, P.; Wüthrich, K. *J. Biomolecular NMR* **1995**, *6*, 1−10.
(22) Wüthrich, K. *NMR of Proteins and Nucleic Acids*; John Wiley and Sons: New York 1986.
(23) Güntert, P.; Mumenthaler, C.; Wüthrich, K. *J. Mol. Biol.* **1997**, *273*, 283−298.
(24) Koradi, R.; Billeter, M.; Wüthrich, K. *J. Mol. Graphics* **1996**, *14*, 51−55.
(25) Güntert, P. *Quart. Rev. Biophys.* **1998**, *31* (2), 145−237.
(26) Nèmethy, G.; Pottle, M. S.; Scheraga, H. A. *J. Phys. Chem.* **1983**, *87*, 1883−1887.
(27) Mohamadi, F.; Richards, N. G. J.; Guida, W. C.; Liskamp, R.; Lipton, M.; Caufield, C.; Chang, G.; Hendrickson, T.; Still, W. C. *J. Comput. Chem.* **1990**, *11*, 440−467.
(28) (a) Weiner, S. J.; Kollman, P. A.; Case, D. A.; Singh, U. C.; Chio, C.; Alagona, G.; Profeta, S.; Weiner, P. *J. Am. Chem. Soc.* **1984**, *106*, 765−784. (b) McDonald, D. Q.; Still, W. C. *Tetrahedron Lett.* **1992**, *33*,7743−7746.

dihedral angle of the carbomethoxy-L-norleucyl unit were allowed to rotate. In addition, a suitable selection of amino acid side chains were also set as rotable in order to assess the role of neighboring residues into the stabilization of the conformation at the PEG−Nle fragment. At least one thousand conformations were sampled per MC CS cycle. Among them, those having an energy (AMBER* force field) not greater than 50 kJ/mol with the respect to the energetically most favorable one were selected, analyzed for local structure and grouped into structurally related families by means of cluster analysis (XCLUSTER software package[29]). Cluster analysis allows to assess whether a given ensemble of conformations could be split into structurally related groupings (clusters) or whether the conformations were distributed in a continuous manner. The conformational distance between a pair of structures was measured by calculating the atomic root-mean-square displacements after best superposition of a suitable selection of heavy atoms. These atomic rms displacements were then used to build up the distance matrix to be searched for clusters.

Results

Conformational Models in TFE Solution. (A) hGRF-(1−29)−NH$_2$. Both one- and two-dimensional ^{1}H NMR spectra of hGRF(1−29)−NH$_2$ showed a single set of signals per amino acid residue, indicating that in TFE solution a single major conformation of the peptide exists or that dynamical processes, if any, must be in the fast exchanging regime. The high content of α-helix structure for hGRF(1−29)−NH$_2$ in TFE solution can be clearly argued by the spreading of the backbone amide proton resonances, which extend over a range 1.5 ppm wide (the chemical shift range for amide protons is reduced to 0.6 ppm in aqueous solution) and by the analysis of the secondary structure shifts, calculated as described in refs 30,32. The secondary structure shifts $\Delta\delta_{ss}$ are plotted against the residue sequence number for H$^\alpha$ and HN protons in Figure 2A and 2B, respectively. Most of the hGRF(1−29)−NH$_2$ H$^\alpha$ protons present an upfield shift with respect to random coil chemical shifts, indicating the predominance of α-helix secondary structure. This can be clearly seen if the chemical shift index (CSI)[30] is calculated (see also Figure 2A). Note that no corrections were made for the intrinsic effect of TFE on the chemical shift (solvent effect not related to structural changes), because this effect has been shown to be negligible for H$^\alpha$.[31,33] It is worth noting that the secondary structure shifts of HN protons show a considerable periodic fluctuation along the sequence, this feature being typical of amphiphilic peptides.[32] Consistently with the high α-helix content estimated by chemical shift analysis, a large number of NOE peaks typical of the α-helix were detected in 2D-NOESY spectra [cross-peaks between sequential HN, between H$^\alpha$(*i*) and H$^\beta$(*i*+*3*); between H$^\alpha$(*i*) and NH(*i*+*4*); between H$^\alpha$(*i*) and NH(*i*+*3*)]. No long-range NOE contacts (i.e., between residues separated by more than four residues in the primary structure) were found, suggesting the presence of a single straight α-helix segment. Further structural details were achieved by means of constrained TAD with simulated annealing calculations. These calculations were initially carried out with geometric constraints obtained from NOESY spectra acquired at 290 K and 300 ms mixing time. NOE build up curves showed that most of the measured NOE peak intensities grew up or leveled off up to a mixing time of 300 ms. For longer mixing times, the intensity of a significant number of NOE peaks began to decrease. At mixing times shorter than 300 ms, spin diffusion effects were negligible. The NOE measurements allowed us to derive a total number of 303 interproton upper limit bounds (Table 2, Figure 3) which were used for structure optimization. One thousand random conformations of hGRF(1−29)−NH$_2$ were generated, optimized by constrained TAD with simulated annealing and ranked according to their residual target functions. The latter parameter describes the quality of a given optimized structure, both in terms of consistency with the experimental constraints and in terms of nonbonded geometry. A sub-ensemble of thirty conformers endowed with lowest residual target function was selected out from the ensemble of final acceptable conformers for further structural analysis and statistics. The average residual target function of the selected conformers had a value of 0.11 ± 0.01 Å^2, indicating that the calculations converged to a family of structures which were highly consistent with the experimental constraints [for a peptide of 29 amino acids, an acceptable value of the residual target function should be 0.56 Å^2 or less (see ref 23)]. The consistency of these models was also indicated by the low number and severity of upper limit bound violations and steric overlap violations. More details about the results of structure optimization are given in Table 2, whereas Figure 4 shows the ensemble of 30 structures after best superposition of backbone segments 2−28, 4−14, and 20−28. Despite the low value of the residual target function, the atomic RMSDs calculated after best superposition of the 30 selected structures over segment 2−28 were quite high for a peptide of this size (backbone and heavy atoms RMSD are 2.24 and 3.57 Å

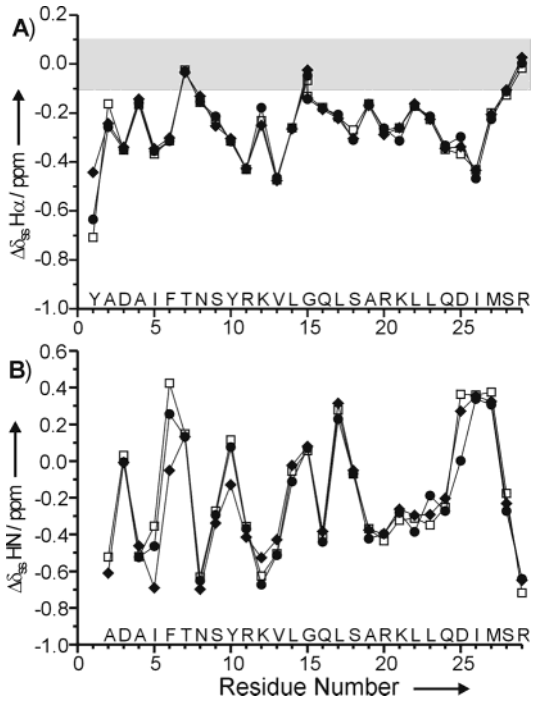

Figure 2. Plot of secondary structure shifts of H$^\alpha$ (A) and HN (B) resonances against residue number for (□) hGRF(1−29)−NH$_2$, (●) Lys^{21}PEG−GRF and (◆) Lys^{12}PEG−GRF. According to the method of Wishart and Sykes for the identification of secondary structure elements [30], $\Delta\delta_{ss}$ values falling within the shaded area in A are assigned to a chemical shift index (CSI) of zero. Secondary structure shifts falling in the areas below and above the shaded area are assigned to index values of −1 and +1, respectively. A cluster of −1 indices (not necessarily consecutive) uninterrupted by a +1 identifies a α-helix element.

(29) Shenkin, P. S.; McDonald, D. Q. *J. Comput. Chem.* **1994**, *15*, 899−916.
(30) Wishart, D. S.; Sykes, B. D. *Methods Enzymol.* **1994**, *239*, 363−392.
(31) Merutka, G.; Dyson, H. J.; Wright, P. E. *J. Biomol. NMR* **1995**, *5*, 14−24.
(32) Szilágyi, L. *Prog. Magn. Res. Spectrosc.* **1995**, *27*, 325−443.

Table 1. Selected ^{1}H NMR Chemical Shifts of hGRF(1−29)−NH_2, Lys^{21}PEG−GRF, and Lys^{12}PEG−GRF in TFE[a]

residue	atom	hGRF(1–29)–NH_2	Lys^{21}PEG–GRF	Lys^{12}PEG–GRF
Tyr1	H^{α}	3.89	3.97	4.16
Ala2	HN (H^{α})	7.73 (4.19)	/ (4.09)	7.64 (4.11)
Asp3	HN (H^{α})	8.44 (4.41)	8.40 (4.41)	8.40 (4.42)
Ala4	HN (H^{α})	7.73 (4.18)	7.73 (4.19)	7.79 (4.21)
Ile5	HN (H^{α})	7.84 (3.86)	7.73 (3.87)	7.50 (3.88)
Phe6	HN (H^{α})	8.65 (4.35)	8.48 (4.35)	8.18 (4.36)
Thr7	HN (H^{α})	8.39 (4.32)	8.37 (4.32)	8.37 (4.32)
Asn8	HN (H^{α})	8.12 (4.59)	8.10 (4.60)	8.05 (4.62)
Ser9	HN (H^{α})	8.11 (4.27)	8.09 (4.29)	8.04 (4.25)
Tyr10	HN (H^{α})	8.30 (4.28)	8.26 (4.28)	8.05 (4.30)
Arg11	HN (H^{α})	7.91 (3.95)	7.90 (3.95)	7.85 (3.95)
Lys12	HN (H^{α})	7.78 (4.13)	7.74 (4.18)	7.88 (4.11)
Val13	HN (H^{α})	7.93 (3.71)	7.93 (3.72)	8.01 (3.70)
Leu14	HN (H^{α})	8.36 (4.12)	8.31 (4.12)	8.40 (4.12)
Gly15	HN (H^{α})	8.45 (3.90/3.84)	8.46 (3.92/3.83)	8.47 (3.95/3.83)
Gln16	HN (H^{α})	8.01 (4.19)	7.97 (4.19)	8.03 (4.18)
Leu17	HN (H^{α})	8.70 (4.16)	8.65 (4.17)	8.73 (4.16)
Ser18	HN (H^{α})	8.31 (4.23)	8.31 (4.19)	8.33 (4.20)
Ala19	HN (H^{α})	7.88 (4.19)	7.83 (4.19)	7.87 (4.18)
Arg20	HN (H^{α})	7.84 (4.11)	7.87 (4.12)	7.88 (4.09)
Lys21	HN (H^{α})	8.09 (4.10)	8.13 (4.05)	8.15 (4.10)
Leu22	HN (H^{α})	8.11 (4.21)	8.04 (4.21)	8.12 (4.22)
Leu23	HN (H^{α})	8.07 (4.15)	8.23 (4.17)	8.13 (4.15)
Gln24	HN (H^{α})	8.16 (4.02)	8.14 (4.04)	8.21 (4.03)
Asp25	HN (H^{α})	8.77 (4.39)	8.41 (4.46)	8.68 (4.42)
Ile26	HN (H^{α})	8.59 (3.80)	8.57 (3.76)	8.58 (3.80)
Met27	HN (H^{α})	8.80 (4.32)	8.73 (4.29)	8.74 (4.31)
Ser28	HN (H^{α})	8.20 (4.37)	8.11 (4.39)	8.15 (4.40)
Arg29	HN (H^{α})	7.55 (4.36)	7.63 (4.38)	7.62 (4.41)
Nle	HN		6.13, 6.08[b]	6.05
	H^{α}		4.06, 4.05[b]	4.02
	$H^{\beta 2}/H^{\beta 3}$		1.63	1.62
	$H^{\gamma 2}/H^{\gamma 3}$		1.77	1.77
	$H^{\delta 2}/H^{\delta 3}$		1.35	1.38
	$H^{\epsilon}{}_3$		0.91	0.91
PEG_{5000}	$-OCH_2-$		3.68	3.68
	$-OCH_3$		3.40	3.40

[a] TFE-d2-OH, $T = 310$ K. Chemical shifts referenced to TMS by using the signal of CF_3CHD-OH at 3.897 ppm as a secondary standard. Assignments are not stereospecific. [b] These hydrogen atoms yielded a double set of resonances. The full listing is available in the Supporting Information.

respectively), indicating that the conformational models were globally not so well-defined. Thus, an analysis for local structure was performed by calculating the atomic RMSDs after superposition of four-residue segments and plotting them against the position in the amino acid sequence (Figure 5). It can be seen that the superposition over segment 16−19 presents a peak in the backbone RMSD value, whereas the remaining segments of the peptide show remarkably low atomic RMSDs (smaller than 0.3 Å, if the residues close to the N-and C-termini are not considered). Thus, the peptide models are poorly defined only in the region encompassing residues 16−19, where many conformations are found which are consistent with the applied constraints. The hGRF(1−29)−NH_2 molecule is found to adopt a well-defined α-helix conformation within segment 4−16 (N-terminus α-helix domain) and segment 18−28 (C-terminus α-helix domain). The conformation of segment 16−19 introduces a kink between the axes of the N-terminus and C-terminus α-helix domains in most of the structures.

To assess whether the poor definition of the central part of the molecule arose from the lack of significant NOE data rather than from the intrinsic lack of secondary structure (brought about, for instance, by conformational flexibility), further NOESY spectra were acquired at higher temperatures (the mixing time was kept fixed at 300 ms). The dataset obtained at 295 K afforded the highest number of NOE contacts, because at this temperature a minimum extent of spectral overlap occurred (especially in the H^{α}/H^{β} and H^{α}/HN region). As a matter of fact, a total of 386 upper limit bounds could be derived, and a significantly higher number of constraints typical of the α-helix conformation was found (Figure 3). Remarkably, the number of correlations involving residues in position *i*, *i+3* almost doubled with respect to that found at 290 K (Table 2). Constrained TAD with simulated annealing calculations were then repeated with the NOE restraints obtained from NOESY spectra acquired at 295 K. This round of calculations was carried out by following the same protocol as described above, and the calculation converged to an ensemble of structures characterized by a very low average residual target function (0.09 ± 0.002 Å^2, calculated over 30 conformers having lowest residual target function). More details about the input constraints and results from structure optimization are listed in Table 2, whereas Figure 4 (right column) shows some backbone superpositions of the 30 structures in which the RMSDs over selected molecular segments have been minimized. These models are globally more defined (backbone and heavy atoms RMSDs over segment 2−28 are 0.63 and 1.32 Å respectively) than the ones obtained from NOE measurements carried out at 290 K. These findings suggest that the α-helix conformation actually spans the whole length of the peptide, and that the definition of the models strongly depends on the completeness and accuracy of the set of NOE derived distances. The view that the single α-helix structure basically spans the whole length of the molecule is consistent with amide protons exchange kinetics (see below).

The results of our investigation are in good agreement with previous studies carried out by means of the combined use of CD and NMR.[15,16] In these studies it was pointed out that the [Nle^{27}]-hGRF(1−29)−NH_2 derivative of hGRF adopted in 30% v/v TFE/water solution a α-helix structure within fragments 6−13 and 16−29 and that the middle part of the molecule could not be uniquely defined because of the lack of significant NOE data. In another study,[13] the structure of hGRF(1−29)−NH_2 in 75% v/v methanol/water solution was reported to consist in a single α-helix straight segment, which however showed a tendency to form kinks near residue 16 and/or 25.

(B) Lys^{21}PEG−GRF. The NMR spectra of Lys^{21}PEG−GRF in TFE solution showed a large spreading of the amide proton resonances (extending over a region about 1.5 ppm wide) and a high number of NOE contacts typical of the α-helix. By contrast, the NOESY spectra obtained in aqueous solution (mixing time 300 ms, $T = 275$ K) showed very severe signal overlap (the amide protons grouped within a spectral region about 0.6 ppm wide) and a limited amount of NOE contacts. The secondary structure shifts of H^{α} and HN protons in TFE solution are also consistent with a high extent of α-helix secondary structure. These shifts are indeed almost identical to those of parent hGRF(1−29)−NH_2 (Figure 2), and indicate that the amphiphilic character of the helix is retained. The sequence specific assignment procedure allowed to unambiguously identify all the resonances of the backbone protons, including the ones belonging to Lys^{21} and Lys^{12}. A number of NOE contacts were detected between the Lys^{21} side chain and Nle (namely, Lys^{21} H^{ζ}/Nle H^{α}, Lys^{21} H^{ζ}/Nle H^{β}, Lys^{21} H^{ζ}/Nle H^{γ}, and Lys^{21} H^{ζ}/Nle HN). Interestingly, the Nle HN proton gave rise to a double set of TOCSY stripes falling at amide proton frequencies

Table 2. Summary of the NOE Derived Constraints used for Torsion Angle Dynamics (TAD) with Simulated Annealing Calculations and Results from Structure Optimization

	hGRF(1–29)–NH$_2$[a]		Lys^{21}PEG–GRF[b]	Lys^{12}PEG–GRF[c]
	T = 290 K	T = 295 K	T = 310 K	T = 310 K
interproton upper distance bounds from NOEs[d]				
total no.	303	386	357	318
intraresidue	149	163	122	114
i, *i*+1	69	83	105	98
i, *i*+2	16	16	21	21
i, *i*+3	48	95	82	66
i, *i*+4	21	29	27	19
i, *i*+5 or more	0	0	0	0
structure calculation				
no of selected conformers[e]	30	30	30	30
final target function (Å^2) [f]	0.11 ± 0.007	0.09 ± 0.002	0.34 ± 0.04	0.14 ± 0.005
violations of upper limit bounds [g]				
violation > 0.2 Å	0	0	0	0
violation > 0.1 Å	2	1	2	11
Violation of van der Waals lower bounds [g]				
violation > 0.1 Å	0	0	1	0
backbone RMSD (Å) ± sd				
segment 2−28	2.24 ± 0.99	0.63 ± 0.23	2.09 ± 1.58	2.62 ± 1.71
segment 4−28	2.22 ± 1.06	0.58 ± 0.22	1.87 ± 1.55	2.53 ± 1.73
segment 4−14	0.29 ± 0.14	0.31 ± 0.22	0.59 ± 0.27	0.32 ± 0.32
segment 14−20	1.29 ± 0.79	0.15 ± 0.07	0.62 ± 0.57	0.62 ± 0.28
segment 20−28	0.30 ± 0.16	0.06 ± 0.03	0.34 ± 0.20	0.34 ± 0.18
heavy atoms RMSD (Å) ± sd				
segment 2−28	3.57 ± 1.55	1.32 ± 0.35	2.73 ± 1.41	3.58 ± 1.94
segment 4−28	3.57 ± 1.62	1.31 ± 0.36	2.60 ± 1.36	3.47 ± 1.88
segment 4−14	1.00 ± 0.32	1.06 ± 0.29	1.52 ± 0.27	1.07 ± 0.40
segment 14−20	2.51 ± 1.25	1.20 ± 0.60	1.61 ± 0.64	1.64 ± 0.39
segment 20−28	1.04 ± 0.24	1.08 ± 0.32	1.46 ± 0.25	1.32 ± 0.22

[a] hGRF(1−29)−NH$_2$ 2.5 mM, TFE-d$_2$−OH, NOESY mixing time 300 ms. [b] Lys^{21}PEG−GRF 0.6 mM, TFE-d$_2$−OH, NOESY mixing time 250 ms. [c] Lys^{12}PEG−GRF 0.6 mM, TFE-d$_2$−OH, NOESY mixing time 250 ms. [d] Number of nontrivial constraints after modification of the upper distance limits that involved diastereotopic atom pairs without stereospecific assignment (as described in ref 25). [e] Selected for statistics and structural analysis out of the ensemble of acceptable minimized conformers. [f] Averaged over all selected conformers, ± sd. [g] Violations consistently found in at least one-third of the accepted structures.

of 6.18 and 6.13 ppm (at 305 K, labeled Nle HN and Nle HN* in Figure 6). Also, two signals were detected for Nle H$^\alpha$ (4.04 and 4.05 ppm) and Lys^{21} H$^\zeta$ (7.21 and 7.18 ppm). The difference in the chemical shifts of the Nle HN proton increased with decreasing the temperature, whereas in aqueous solution (at 275 K) a single set of signals was found for both Nle NH and Lys^{21} H$^\zeta$ (falling at 7.37 and 8.33 ppm respectively). All of these findings suggest that two slowly interconverting conformers of Lys^{21}PEG−GRF exist likely differing in the conformation at the Nϵ−[norleucyl]−Lys^{21} moiety. Aside from the Nle−Lys^{21} moiety, all the other residues showed a single set of signals. The NOESY spectrum acquired at 310 K with a mixing time of 250 ms allowed us to derive as many as 357 constraints to be used for TAD calculations. Structure optimization was carried out with the same protocols described for native hGRF(1−29)−NH$_2$ (the PEG−Nle moiety was not explicitly included in the calculation). The calculations converged into an ensemble of structures characterized by an average residual target function of 0.34 ± 0.04 Å^2 and backbone and heavy atoms RMSDs of 2.09 and 2.73 Å respectively (RMSDs calculated over segment 2−28). The structure of Lys^{21}PEG−GRF presents a single α-helix domain, which extends over the whole length of the peptide, but the axis of the α-helix is slightly bent. Consistently, several hydrogen bonds typical of the α-helix conformation were found spanning from residue Phe^6 to residue Arg^{29}. The backbone RMSD values calculated over selected molecular segments point out that the α-helix is best defined in region 14−27 rather than in the N-terminus domain (whose helical core encompasses residues 4−12), and that the local conformation in the segment connecting the middle part of the peptide is less clearly defined (Figure 7, left column). This is not surprising, because it has been shown that the completeness and accuracy of the NOE measurements is critical to obtain a high definition of the structure especially around the central part of the peptide. In the case of the PEGylated analogues, such an accuracy is very difficult to be reached because the very intense resonance of the PEG methylene groups (falling at about 3.4 ppm) introduces a remarkable t_1 noise in NOESY spectra, which prevents the accurate measurement (or detection) of a significant number of NOE peaks (mostly the ones due to H$^\alpha$/H$^\beta$ correlations). Presaturation of the ^{1}H NMR line of PEG ethyleneglycol groups has only a marginal effect in the minimization of such t_1 noise. On the basis of the comparison between the backbone conformations of hGRF(1−29)−NH$_2$ and Lys^{21}PEG−GRF, it can be concluded that the two peptides are very similar. The PEG moiety does not interfere with the tendency of the peptide to adopt the α-helix structure, since residue Lys^{21} is invariably included within well-defined α-helix regions both in hGRF-(1−29)−NH$_2$ and Lys^{21}PEG−GRF. This finding is rather unexpected, because the introduction of the PEG moiety was envisaged to appreciably modify the chemical environment or the molecular flexibility at least nearby residue Lys^{21}. Rather, the peptide moiety induces some conformational rigidity at the PEG−Nle junction, as witnessed by the fact that this molecular

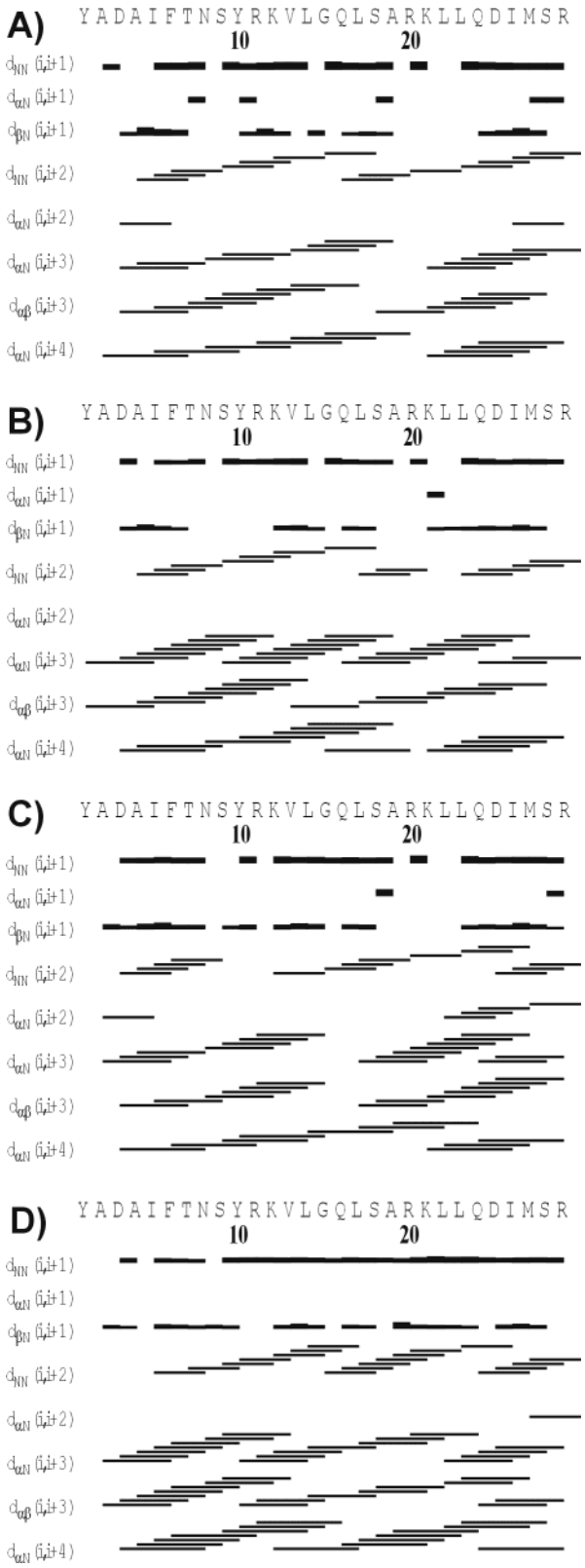

Figure 3. Sequential and medium range ^{1}H-^{1}H NOE contacts observed in the NOESY spectra (TFE solution) for (A) hGRF(1−29)−NH_2 (T = 290 K, NOESY mixing time 300 ms); (B) hGRF(1−29)−NH_2 (T = 295 K, NOESY mixing time 300 ms); (C) Lys^{12}PEG−GRF (T = 310 K, NOESY mixing time 250 ms); and D) Lys^{21}PEG−GRF (T = 310 K, NOESY mixing time 250 ms).

segment is blocked into two slowly interconverting conformations. Thus, the peptide may be envisaged to behave as a quite rigid body, whereas the Nle side-chain is endowed with higher local mobility.

To gain further insights into the conformation of the Lys^{21}/Nle junction, a series of Monte Carlo Conformational Search (MC CS) calculations was performed. The dihedral angles to be rotated in these calculations were chosen according to the following lines.

(i) The polymeric PEG unit was assumed to be very flexible, and modeled by a simple methoxy group to reduce the number of rotable torsion angles.

(ii) The double set of signals found for the HN and H$^\alpha$ protons of Nle and for the H$^\zeta$ one of Lys^{21} indicated that the site which is involved in conformational isomerism is located at the junction between the Lys^{21} side chain and Nle. Although a possible explanation may be cis−trans isomerism at the amide and/or carbammic bonds, the very small chemical shift differences between the two conformers make this hypothesis very unlike. Thus, CS calculations were performed in the hypothesis of trans geometries at the amide and carbammic bonds, whereas all the dihedral side chain χ angles of Lys^{21} and all the ϕ, ψ, and χ angles of Nle were set as rotable. In addition, free rotation around the carbammic (CO)−(OCH_3) bond was imposed.

(iii) The backbone conformation of Lys^{21}PEG−GRF was assumed to be rigid, and a representative structure selected out of the bundle of structures obtained by TAD was taken as the starting conformation.

(iv) Isomerism at the Lys−Nle moiety is observed for Lys^{21}PEG−GRF but not for Lys^{12}PEG−GRF (see below), indicating that the source of conformational isomerism must be related to the network of interactions between side chain of Lys^{21} and those of the closely spaced residues (according to the periodicity of the α-helix). In this regard, the inspection of the structures coming from TAD calculations indicated that Arg^{20}, Gln^{24}, Asp^{25}, and Arg^{29} had the highest probability to form a network of dipolar or charge−charge interactions with Lys^{21}. All of the side chain χ angles of those residues were initially set as rotable.

The first round of MC CS was performed by sampling one thousand conformations, among which the ones endowed with energies not higher than 50 kJ/mol with respect to the lowest energy conformer were analyzed for structural similarity. Such analysis was done by cluster analysis, where the conformational distance between pairs of structures was measured by calculating the atomic root-mean-square displacements after best superposition of a suitable selection of heavy atoms. Namely, structural similarity was assessed on the basis of the best superposition over the heavy atoms of Lys^{21}, Nle, PEG, Asp^{25}, Ser^{28}, and Arg^{29}. This round of calculations afforded an ensemble of 91 low energy conformers that could not be clearly clustered into two well-defined families of conformers on the basis of the conformation at the Nle−Lys^{21} moiety. Although the obtained structures did not provide a clear picture of the local conformers, these calculations clearly indicated that Asp^{25} and Arg^{29} side chains were specifically involved into a ion pairing interaction. More generally, all the MC CS simulations where the side chain dihedral angles of Asp^{25} and Arg^{29} were set free to rotate showed that the Asp^{25} carboxyl group moved toward the Arg^{29} guanidino group, whereas the distance between Asp^{25} carboxyl group and Lys^{21} slightly increased. The distances involving Asp^{25} were however still compatible with the NOE-derived upper limit

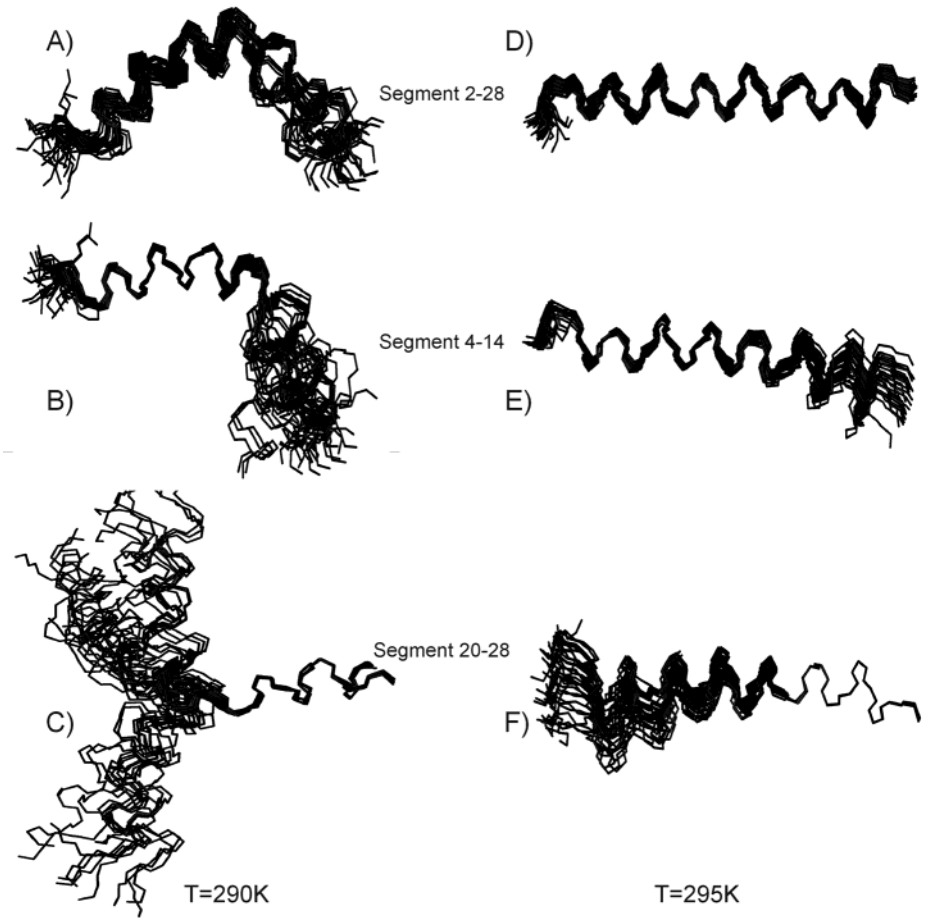

Figure 4. Superposition of thirty structures of hGRF(1−29)−NH_2 (TFE solution) obtained by restrained TAD with simulated annealing. The structures in A, B and C were obtained from NOE measurements carried out at 290 K (NOESY mixing time 300ms); the structures in D, E, and F are from NOE measurements carried out at 295 K (NOESY mixing time 300 ms). The atomic RMSD has been minimized over segment 2−28 (A,D), segment 4−14 (B, E), and segment 20−28 (C,F). The C-terminus is on the right.

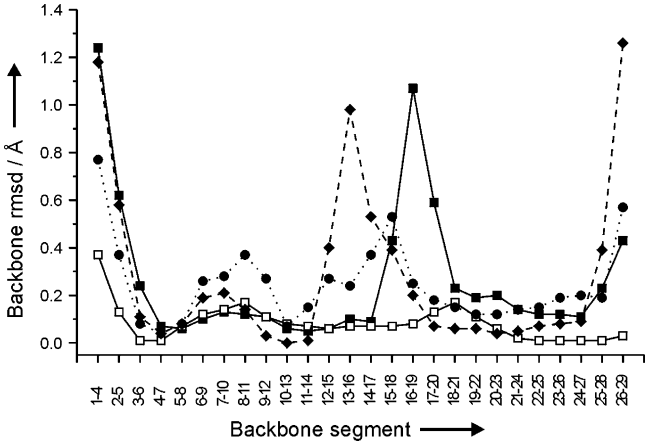

Figure 5. Plot of the atomic backbone RMSDs calculated over the superposition of consecutive four-residue segments versus the position of the segment in the amino acid sequence. The RMSDs were calculated over superposition of thirty structures. ■ hGRF(1−29)−NH_2 [structures from NOE measurements carried out at 290 K]; □ hGRF(1−29)−NH_2 [structures from NOE measurements carried out at 295 K]; ● Lys^{21}PEG−GRF (310 K); ◆ Lys^{12}PEG−GRF (310 K).

bounds. Thus, the side chain of Arg^{29} was kept fixed in the conformation giving rise to the ion-pairing with Asp^{25} to reduce the number of rotable bonds in further calculations and to increase the accuracy in the sampling of the conformational space allowed for PEG−Nle and for the side chains of Lys^{21}, Arg^{20}, Gln^{24}, and Asp^{25}. The MC CS calculations carried out in this way afforded an ensemble of 77 structures (selected out of 1000 generated conformers). The analysis for local conformations at the Nle−Lys^{21} fragment and at the side chains of the residues which were left free to rotate revealed the presence of two major families (family 1, 29 structures out of 77; family 2, 27 structures out of 77). The remaining conformers (21 out of 77) did not fall into a well-defined family of structures. The two main families have very similar average energies and share the following features: (i) the side chain of Nle shows no conformational restrictions, whereas the side chains of Lys^{21}, Arg^{20}, Gln^{24}, and Asp^{25} show very limited degrees of freedom because of steric hindrance brought about by the α-helix packing and because of extensive hydrogen bonds; (ii) a strong hydrogen bond is found between Nle CO and the side chain guanidino hydrogens of Arg^{20}; and (iii) the Nle HN is not involved in any hydrogen bond interaction. These two families show a significant difference in the conformation of the ψ dihedral angle of Nle and in the hydrogen bonding network involving residues Arg^{20}, Gln^{24}, and the Nle CO/carbammic CO of the PEG−Nle fragment (Figure 8). These models may provide a reasonable explanation for the experimental findings, even though other conformational possibilities for the Nle−Lys^{21} fragment may be envisaged. As a matter of fact, the calculations were carried out under strong

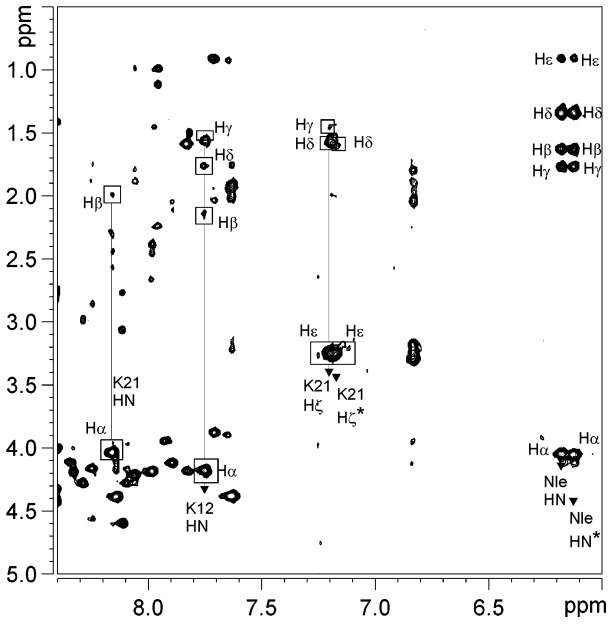

Figure 6. Expansion of the 2D-TOCSY spectrum of Lys[21]PEG−GRF in TFE-d_2−OH solution (3.86 mg/mL, 305 K, isotropic mixing time 100 ms) showing the fingerprint region (F_2 8.4−6.0 ppm, F_1 5.0−0.5 ppm). The amide TOCSY stripes from Lys[12] HN, Lys[21] HN, Lys[21] Hζ, and Nle HN are shown. Note that Lys[21] Hζ and Nle HN give rise to two separate signals (marked with asterisks), indicating the presence of two local conformations at the Lys[21]−Nle fragment.

approximations (for instance, no contribution of TFE solvation, that may be important to determine the conformational preferences, was taken into account). The important information which can be derived from CS calculations is that the peptide side chains around Lys[21] give rise to a rigid and compact surface, in which the charged residue of Arg[20] provides a favorable point of anchorage to the carbammic group belonging to the PEG−Nle moiety.

(C) Lys[12]PEG−GRF. The 2D-NMR spectra of Lys[12]PEG−GRF in TFE solution basically revealed the same features as found for the Lys[21]PEG−GRF derivative. Lys[12]PEG−GRF is endowed with a high content of α-helix secondary structure, as far as estimated from secondary structure shifts (Figure 2), spreading of the backbone amide resonances, number and quality of sequential and medium range NOE peaks (Figure 3). A number of NOE contacts between the side chain protons of Lys[12] and the Nle ones could be unambiguously detected (namely, Lys[12] H^{ζ}/Nle H^{α} and Lys[12] H^{ζ}/Nle HN). Unlike the case of Lys[21]PEG−GRF, no evidence for conformational isomerism at the Nle−Lys[12] moiety was found, because the Lys[12] H^{ζ} and Nle HN protons gave rise to a single set of resonances. Structure calculations were carried out following the same protocol as described for the Lys[21]PEG−GRF analogue. As many as 318 upper limit distance constraints were derived from a NOESY spectrum acquired at 310 K with a mixing time of 250 ms. The sub-ensemble comprising the best 30 energy minimized conformers was characterized by an average target function of 0.14 ± 0.005 Å^2, and by backbone and heavy atom RMSD of 2.62 and 3.58 Å respectively (calculated over segment 2−28). The optimized conformers show two well-defined α-helix domains in the segments 4−14 and 18−28 (Figure 7, right column). Segment 15−17 is not uniquely defined by the NOE constraints, and consistently the local atomic RMSD show a peak in the region 13−16 (Figure 5). Thus, the Lys[12]PEG−GRF molecule retains the strong tendency to form α-helix secondary structures whose cores are located in the fragment 4−14 (N-terminus α-helix domain) and in the fragment 18−28 (C-terminus α-helix domain). As in the case of Lys[21]PEG−GRF, the local conformation in the middle tract of the molecule could not be uniquely defined because spectral crowding and t_1 noise hampered the detection of a significant number of H^{α}/H^{β} correlations. It is worth noting that the Lys[12] residue which has been selectively conjugated to PEG is found in a well-defined backbone conformation within a molecular segment endowed with α-helix structure.

Exchange Kinetics of Labile Protons (TFE-d_3) and Amide Temperature Coefficients. Further insights into the stability and extent of the α-helix domains can be obtained by the analysis of the exchange kinetics between the peptide labile protons (basically amide protons) and the alcoholic proton of TFE. A series of one-dimensional ^{1}H NMR spectra were acquired (T = 310 K) at different times after dissolution of the peptides into fully deuterated TFE. Two-dimensional NOESY and TOCSY spectra were also acquired (typically after 250 and 1100 min since the beginning of the hydrogen exchange experiment) in order to aid resonance assignment in crowded spectral regions.

The backbone amide protons were grouped into three classes according to their pseudo first-order kinetic exchange rates: (i) amide protons showing complete exchange immediately after addition of the solvent ($k_{ex} > 2 \times 10^{-1}$ min^{-1}) (ii) amide protons showing intermediate exchange rates (signals decaying within 1500 min since dissolution, 2.5×10^{-2} min$^{-1} < k_{ex} < 2 \times 10^{-1}$ min^{-1}) and (iii) amide protons showing very slow exchange (signal still detected after 1500 min, $k_{ex} < 2.5 \times 10^{-2}$ min^{-1}). The comparison of kinetic data for hGRF(1−29)−NH_2 and its PEGylated analogues (summarized in Table 3) leads to the following observations. For all the considered compounds, the amide proton exchange rates decrease in a continuous way on going from the N-terminus to the C-terminus. Amide protons belonging to the C-terminus domain (mainly Met[27], Ile[26], Gln[24], Leu[23], and Leu[22]) are endowed with remarkably slow exchange kinetics in both hGRF(1−29)−NH_2 and the PEGylated analogues. Then, it can be concluded that the α-helix structure is more rigid in the C-terminus region than close to the N-terminus. Remarkably, the slowest exchanging HN is the one belonging to Met[27]. This amide hydrogen is invariably found to be hydrogen bound to Leu[23] CO in the molecular models [both of hGRF(1−29)−NH_2 and of the PEGylated analogues]. The low stability of the α-helix secondary structure in the N-terminus domain with respect to the C-terminus one is not unexpected because Ser[9] and Thr[7] side chain hydroxyl groups can interfere with the formation of a proper α-helix hydrogen bond network and because amide protons belonging to the N-terminus cap lack of proper stabilizing hydrogen bond interactions. As far as can be deduced from the intermediate exchange rates in the middle part of the peptide, this peptide segment must also be well-structured. This finding supports the view that the poor definition of the middle part of the peptide often encountered in the molecular models is due to the lack of significant NOE information rather than to an intrinsic tendency to adopt a disordered conformation. The relatively slow exchange kinetics observed for Leu[14] and Leu[17] amide protons suggest that such

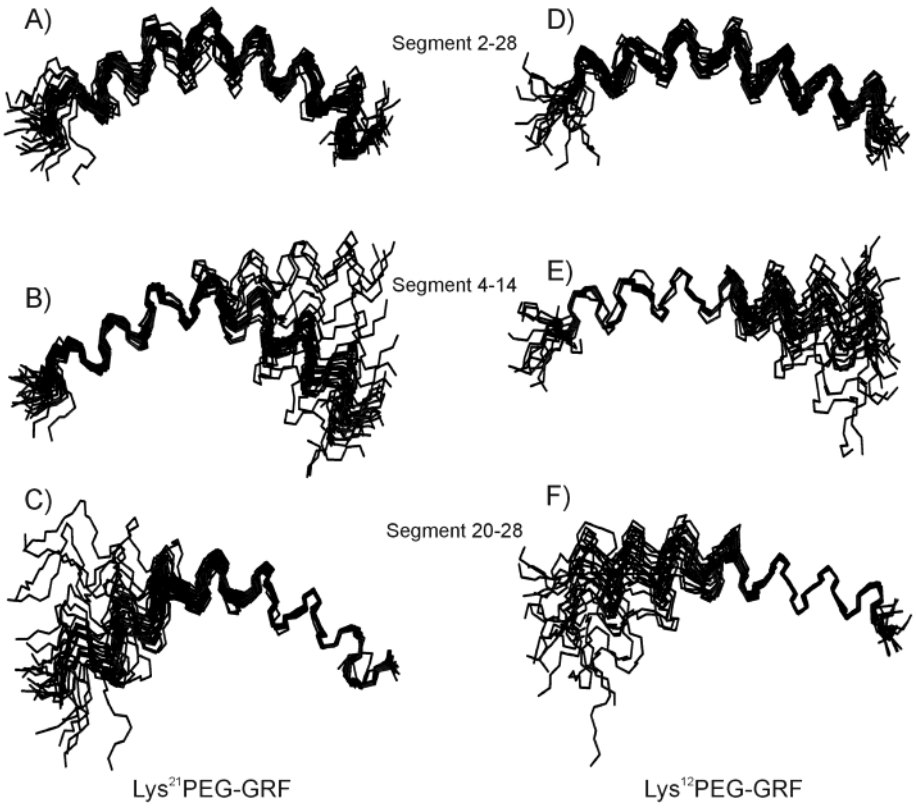

Figure 7. Superposition of thirty structures of Lys^{21}PEG−GRF (A,B,C) and Lys^{12}PEG−GRF (D,E,F) in TFE solution obtained by restrained TAD with simulated annealing. The atomic RMSD has been minimized over segment 2−28 (A,D), segment 4−14 (B, E) and segment 20−28 (C,F). The C-terminus is on the right.

residues may have a pivotal role in the stabilization of the secondary structure motifs in the central part of the molecule.

The temperature dependence of the chemical shifts of the backbone amide protons provides fine details about the organization of the α-helix of hGRF(1−29)−NH$_2$ and PEGylated analogues. Figure 9 shows a plot of the temperature coefficients of amide protons ($\Delta\delta/\Delta T$) versus the position of the residue along the amino acid sequence. The temperature coefficients show a clear periodic variation along the sequence, in particular within molecular segment 5−20. The temperature coefficient plots for hGRF(1−29)−NH$_2$ and Lys^{12}PEG−GRF are virtually superposable to that of the unmodified peptide along the whole length of the peptide. The amplitude of the oscillations observed for Lys^{21}PEG−GRF is slightly larger, but the periodicity of the oscillations is exactly the same as for hGRF(1−29)−NH$_2$ and Lys^{12}PEG−GRF. For all three compounds, residues Ile^5, Ser^9, Lys^{12}, Gln^{16}, Ala^{19}, and Leu^{23} show maximal $\Delta\delta/\Delta T$ values, whereas residues Thr^7, Tyr^{10}, Leu^{14}, Leu^{17} Lys^{21}, and Met^{27} show minimal $\Delta\delta/\Delta T$ values. The frequency of the variation of $\Delta\delta/\Delta T$ coefficients matches the periodicity of the α-helix structure, with residues showing maximal and minimal $\Delta\delta/\Delta T$ values being on opposite sides of the α-helix cylinder (Figure 10). A similar kind of periodicity is observed if the secondary structure chemical shift of the amide protons at a single temperature are plotted against the sequence (Figure 2B). However, secondary shift oscillations are somewhat reduced in the C-terminus portion of the molecule (segment 20−25). The periodic variation of secondary structure shifts and amide proton temperature coefficients is typical of amphiphilic peptides,[32,33] such as hGRF(1−29)−NH$_2$ has been proposed to be.[11,12,] Therefore, $\Delta\delta/\Delta T$ coefficients and $\Delta\delta_{ss}$ shifts can be used to probe the amphiphilic organization of the peptide α-helix. On this basis, it can be inferred that segment 5−20 of hGRF(1−29)−NH$_2$ has a more pronounced amphiphilic character than the C-terminus one. As far as estimated from molecular models, the partial loss of amphiphilicity in the latter molecular segment is due to the fact that Lys^{21} and Asp^{25}, extending along the hydrophobic α-helix side, break the clustering of apolar residues. The high similarity of $\Delta\delta/\Delta T$ coefficients and $\Delta\delta_{ss}$ shifts between hGRF(1−29)−NH$_2$ and the PEGylated analogues indicate that the amphiphilic organization of the side chains of the parent peptide is basically retained in the PEGylated analogues.

Discussion

The effect on peptide conformation induced by the site-specific PEGylation of hGRF(1−29)−NH$_2$ can be discussed on the basis of four kinds of experimental evidences, namely (i) molecular models obtained from NOE measurements, (ii) exchange kinetics of the amide protons, (iii) secondary structure shifts, and (iv) temperature dependence of the amide proton chemical shifts ($\Delta\delta/\Delta T$ coefficients). The molecular models obtained from NOE measurements support the view that hGRF-(1−29)−NH$_2$, Lys^{21}PEG−GRF and Lys^{12}PEG−GRF share a remarkably similar pattern of secondary structure, all three compounds adopting a α-helix conformation which essentially spans the whole length of the peptide. Although the optimized

(33) Fregeau Gallager, N. L.; Sailer, M.; Niemczura, W. P.; Nakashima, T. T.; Stiles, M. E.; Vederas, J. C. *Biochemistry* **1997**, *36*, 15 062−15 072.

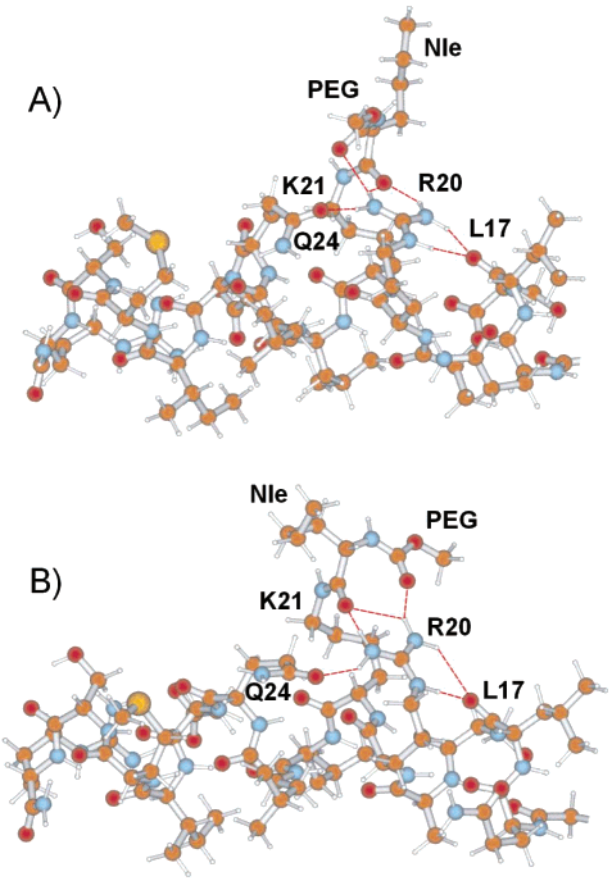

Figure 8. Representative structures of the two major families revealed by cluster analysis on structures obtained by MC CS calculations (Arg^{20}, Lys^{21}, Gln^{24}, Asp^{25} side chain, Nle and carbammic dihedral angles were set as rotable). The peptide segment Gln^{16}-Arg^{29} is shown, the C-terminus is on the left. Hydrogen bonds involving Arg^{20}, PEG, and Nle are shown in red.

models of hGRF(1−29)−NH_2 and its mono-PEGylated analogues show some differences in the local definition around the central part of the peptide, these differences are not believed to be significant, since the quality of the optimized models was found to be strongly dependent upon the accuracy and completeness of the set of NOE-derived distances. The substantial conformational similarity between hGRF(1−29)−NH_2 and its PEGylated analogues in the central molecular segment is well supported by hydrogen/deuterium exchange kinetics. The exchange rates of the amide protons in the middle peptide region have intermediate values with respect to those of residues belonging to the N-terminus and C-terminus α-helix domains, probing the presence of extensive hydrogen bond interactions both for hGRF(1−29)−NH_2 and its PEGylated analogues. The systematic decrease of the exchange rates along the peptide backbone clearly indicates that the α-helix becomes increasingly stable on going from the N-terminus to the C-terminus. Finally, the periodic fluctuations of $\Delta\delta/\Delta T$ coefficients and secondary structure shifts along the amino acid sequence indicate that the GRF α-helix is endowed with a marked amphiphilic character, which is retained in the PEGylated analogues. The amplitude of the fluctuations of H^{α} and HN secondary structure shifts indicate that the amphiphilicity is more pronounced in segment 5−20, whereas it is somewhat attenuated in the adjacent C-terminus segment. Since the plots of $\Delta\delta/\Delta T$ and $\Delta\delta_{ss}$ against the amino acid sequence are very similar for hGRF(1−29)−NH_2 and the PEGylated analogues, the orientation of the side chains with respect to the α-helix axis should be essentially the same in all three peptides. It is noteworthy that both Lys^{12} and Lys^{21} in the hGRF(1−29)−NH_2 molecule are invariantly enclosed into well-defined α-helical domains, and that the introduction of the PEG unit at each of those sites does not alter the local secondary structure or mobility. Rather, the tightness of the packing of the amino acid side chains within the α-helix structure limits the degree of conformational freedom allowed for the Nle−Lys moiety in compound Lys^{21}PEG−GRF, as witnessed by the fact that the Nle spacer is blocked into two slowly interconverting conformations. Lys^{21} is surrounded by a compact surface, in which the functional groups of Arg^{20} and Gln^{24} can provide privileged low energy sites for dipolar interactions with the carbamic group of the PEG−Nle segment (Figure 8). Interestingly, conformational isomerism is observed for Lys^{21}PEG−GRF but not for Lys^{12}PEG−GRF. This fact well correlates with the observed higher degree of freedom found for the Lys^{12} side chain with respect to Lys^{21}, basically arising from different sterical hindrance at the two lysine residues. Such a difference is due to the fact that the position *i+3* relative to Lys^{12} is occupied by a glycine residue, whereas the corresponding position is occupied by a glutamine residue in the case of Lys^{21}.

The finding that PEGylation of hGRF(1−29)−NH_2 does not introduce major changes in the tendency of the peptide to form α-helix structures allows us to exclude any structural contribution to the mechanisms underlying the PEGylation dependent loss of bioactivity observed in the Lys^{12}PEG−GRF derivative. Thus, for such compound, poor bioactivity must be related to hindered binding to the receptor. In this view, site specifically PEGylated peptides can be used to probe the accessibility of the receptor binding domains, and ultimately to get insights into the topology of the ligand/receptor bimolecular complex. In this regard, very little high-resolution structural information is currently available because of the complexity and poor crystallization properties of the GRF receptor. The hGRF receptor (GRF−R) is an integral membrane protein that belongs to the superfamily of G-Protein Coupled Receptors (GPCR), family B, group III (GPCR B−III).[34,35] These receptors are composed by seven transmembrane-spanning α-helical domains connected by alternating intracellular and extracellular loops, with the N-terminus tail located on the extracellular side and the C-terminus on the cytoplasmatic side. Although X-ray diffraction coupled with theoretical methods may provide a model for the topological orientation of the seven transmembrane helices,[36] little is known about the functional conformation of the extracellular loops, which have been shown to be essential for molecular recognition.[35] The localization of the ligand binding domain of the hGRF receptor has been achieved by mutagenesis studies and by analysis of chimeric receptor proteins. These studies pointed out that the N-terminus domain is necessary but not sufficient for ligand binding, and that the extracellular loop regions provide critical determinants for specificity and high affinity binding.[35] More insights into the interaction between hGRF(1−29)−NH_2 and its receptor can be obtained by com-

(34) Gether, U. *Endocrine Reviews* **2000**, *21(1)*, 90−113.
(35) DeAlmeida, V. I.; Mayo, K. E. *Molecular Endocrinology* **1998**, *12*, 750−765.
(36) *Structure−Function Analysis of G Protein-Coupled Receptors*; Wess, J., Ed.; Wiley-Liss, New York, 1999.

Table 3. Exchange Rate Constants for the Backbone Amide Protons of hGRF(1−29)−NH$_2$, Lys^{21}PEG−GRF and Lys^{12}PEG−GRF[a]

	slow exchange	intermediate exchange	fast exchange
hGRF(1−29)−NH$_2$	M^{27}, I^{26}, Q^{24}, L^{23}	R^{29}, S^{28}, L^{22}, K^{21}, R^{20}, L^{17}, G^{15}, L^{14} V^{13}	D^{25}, A^{19}, S^{18}, Q^{16}, K^{12}, R^{11}, Y^{10}, S^{9}, N^{8}, T^{7}, F^{6}, I^{5}, A^{4}, D^{3}, A^{2}
Lys^{21}PEG−GRF	M^{27}, I^{26}, Q^{24}, L^{23}, L^{22}, K^{21}, L^{14}	R^{29}, S^{28}, R^{20}, A^{19}, S^{18}, L^{17}, Gly^{15}	D^{25}, Q^{16}, V^{13}, K^{12}, R^{11}, Y^{10}, S^{9}, N^{8}, T^{7}, F^{6}, I^{5}, A^{4}, D^{3}, A^{2}
Lys^{12}PEG−GRF	M^{27}, I^{26}, Q^{24}, L^{23}, L^{22}, K^{21}, L^{17}, Q^{16}, G^{15}, L^{14}, R^{11}, (K^{12}/R^{20})[b]	R^{29}, S^{28}, A^{19}, S^{18} (V^{13}/Y^{10}/S^{9}/N^{8})[b]	D^{25}, T^{7}, F^{6}, I^{5}, A^{4}, D^{3} A^{2}

[a] The exchange experiments were carried out at 310 K in neat TFE-d$_3$. The k_{ex} have been estimated according to a pseudo first-order kinetic equation. [b] Signal envelope.

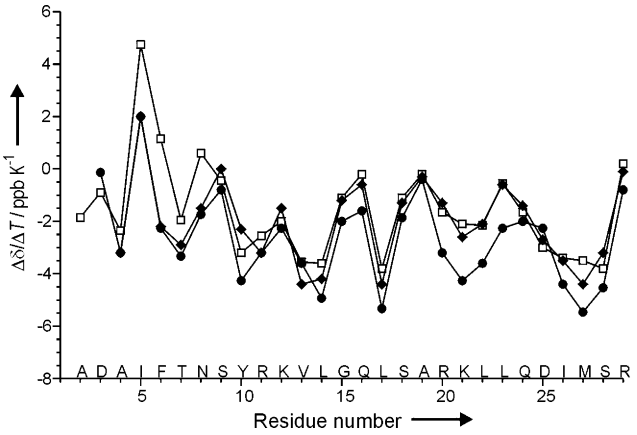

Figure 9. Temperature coefficients of the amide protons ($\Delta\delta/\Delta T$) versus the position of the residue in the amino acid sequence (measured in TFE-d$_2$−OH). □ hGRF(1−29)−NH$_2$; ● Lys^{21}PEG−GRF; ◆ Lys^{12}PEG−GRF.

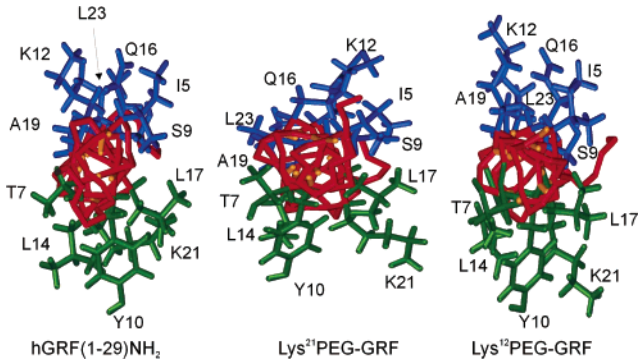

Figure 10. Top view of the α-helix of hGRF(1−29)−NH$_2$, Lys^{21}PEG−GRF and Lys^{12}PEG−GRF showing the orientation of the side chains of those residues that have minimal (green) and maximal (blue) values of $\Delta\delta/\Delta T$ coefficients (shown in Figure 9). The backbone trace of the molecule is colored in red, with the N-terminus side of the α-helix oriented toward the reader.

bining the structural data herein presented with those regarding the relative biological potencies of hGRF(1−29)−NH$_2$ and the mono-PEGylated derivatives. In the ensuing discussion, two simplifications have been done. First, it is assumed that hGRF-(1−29)−NH$_2$ and analogues essentially maintain the α-helix conformation in the receptor-bound form. This assumption is justified by the finding that (i) hGRF(1−29)−NH$_2$ analogues whose α-helix structure has been somehow stabilized show increased binding affinity and (ii) the α-helix structure ensures amphiphilicity, which has been proposed to be important for high affinity binding.[11,12] Second, it is assumed that the potency of the PEGylated analogues (as far as measured by in vitro assays) is directly proportional to the receptor binding affinity. Poor bioactivity is taken as an evidence for low binding affinity, whereas a bioactivity similar to that of the un-PEGylated compound is taken as an evidence for the formation of proper ligand/receptor intermolecular contacts. Under these simplifications, we can evaluate the chemical environment at the lysine residues in the complex between hGRF(1−29)−NH$_2$ and its receptor. The Lys^{21}PEG−GRF analogue has been reported to have a receptor binding affinity comparable to that of hGRF-(1−29)−NH$_2$, whereas for Lys^{12}PEG−GRF a decrease in the binding affinity may be seen.[4] In other studies,[6,7] a number of mono-PEGylated analogues of [Ala^{15}]-hGRF(1−29)−NH$_2$ has been synthesized and assessed for in vitro bioactivity. It has been reported that PEGylation at Lys^{21}, Asp^{25} or at the C-terminus did not significantly affect biological activity, whereas PEGylation at Lys^{12} or Asp^{8} greatly reduced the bioactivity and such reduced bioactivity was correlated with an increasing molecular weight of the PEG moiety, whereas substitution of the PEG unit with acetyl or ethylamido groups at Lys^{12} and Asp^{8} respectively did not significantly affect the potency in comparison with endogenous GRF. The dependence of the biological potency with the molecular weight of PEG in the Lys^{12} PEGylated derivatives indicates that they cannot properly bind to the receptor because of sterical hindrance rather than because of the blockage of specific functional groups. Thus, the PEG group hampers the proper fit of the GRF molecule within the receptor contact sites, indicating that Lys^{12} must fit into a relatively narrow receptor binding pocket, and must be either oriented toward the cellular membrane or toward a receptor domain. On the other hand, the Lys^{21} PEGylated derivatives do bind (and activate) the receptor irrespective of the molecular weight of the PEG unit, suggesting that Lys^{21} falls within a less hindered region. Thus, the orientation of the PEG unit within the ligand/receptor complex does not produce steric overlap with the receptor loops or with the cell membrane. It is worth noting that in all three compounds considered in this work, the two lysine residues extend along almost opposite directions because of the periodicity of the α-helix (Figure 10). It is then apparent that if one of the lysine residues points toward the membrane, the other one must extend toward the extracellular space. Alternatively, both lysines may lie approximately parallel to the membrane, but along opposite directions. Thus, it is concluded that in the bimolecular hGRF(1−29)−NH$_2$/receptor complex Lys^{21} must be oriented toward the extracellular space whereas Lys^{12} toward the cell membrane. Alternatively, Lys^{21} lies parallel to the cell membrane in a region devoid of receptor segments, whereas Lys^{12} lies in the opposite direction,

but making closer contacts with the receptor extracellular domains.

To the best of our knowledge, this is the first work dealing with the high-resolution structural characterization of a PEGylated peptide. Hence, it is worth considering whether the structural results obtained for PEGylated hGRF analogues can be generalized to other bioactive peptides or proteins. Native hGRF(1−29)−NH_2 is characterized by a conformation which lacks stabilizing tertiary structure interactions and whose secondary structure is intrinsically not very stable (indeed secondary structure motifs have to be stabilized by the use of structure promoting solvents to allow for detailed NMR or CD analyses). Nevertheless, site specific PEGylation has no detrimental effects on its conformation. Thus, it can be predicted that the insertion of PEG groups into more structured biomolecules (such as proteins, whose fold is stabilized by tertiary or quaternary structure interactions) will not affect in a significant manner their bioactive conformation. In conclusion, our work suggests that the PEGylation strategy can be applied to more structured biomolecules without causing any structure-dependent loss of intrinsic potency, provided that no specific interaction site is blocked.

List of Abbreviations. PEG: monomethoxypoly(ethyleneglycol) [the subscript denotes the average molecular weight in Da units]; **hGRF:** human Growth Hormone-Releasing Factor; **hGRF(1−29)−NH_2** human Growth Hormone Releasing Factor, fragment 1−29, carboxy-amidated [Tyr^1-Ala^2-Asp^3-Ala^4-Ile^5-Phe^6-Thr^7-Asn^8-Ser^9-Tyr^{10}-Arg^{11}-Lys^{12}-Val^{13}-Leu^{14}-Gly^{15}-Gln^{16}-Leu^{17}-Ser^{18}-Ala^{19}-Arg^{20}-Lys^{21}-Leu^{22}-Leu^{23}-Gln^{24}-Asp^{25}-Ile^{26}-Met^{27}-Ser^{28}-Arg^{29}-NH_2.]; **Lys^{12}PE**G−G**RF:** Nϵ-[monomethoxypoly(ethyleneglycol)norleucyl]Lys^{12}-hGRF(1−29)−NH_2; **Lys^{21}PE**G−G**RF:** Nϵ-[monomethoxypoly(ethyleneglycol) norleucyl]Lys^{21}-hGRF(1−29)−NH_2 **CD:** Circular Dichroism; **NMR:** Nuclear Magnetic Resonance; **MALDI:** Matrix Assisted Laser Desorption Ionization; **TOF:** Time Of Flight; **2D-TOCSY:**TOtal Correlation SpectroscopY; **NOE:** Nuclear Overhauser Effect; **2D-NOESY:** Nuclear Overhauser Effect SpectroscopY; **2D-DQF−COSY:**Double Quantum Filtered COrrelation SpectroscopY; **PFG:** Pulse Field Gradient; **TPPI:** Time Proportional Phase Increment; **RMSD:** Root Mean Square Deviation; **TAD:** Torsion Angle Dynamics; **MM:** Molecular Mechanics; **MC CS:** Monte Carlo Conformational Search; **Nle:** Norleucine; **Aib:** α-aminoisobutyric acid; **Sar:** Sarcosine; **TFE:** 2,2,2-Trifluoroethanol; **TMS:** Tetramethylsilane.

Supporting Information Available: Full listing of ^{1}H NMR chemical shifts and assignment (Table A1); listing of all the upper limit distances used to obtain the molecular models of hGRF(1−29)−NH_2 (Table B1), Lys^{12}PEG−GRF (Table B2), and Lys^{21}PEG−GRF (Table B3).This material is available free of charge via the Internet at http://pubs.acs.org.

JA021264J